



# Ultra-narrow band perfect absorber for sensing applications in the visible region

Ritika Ranga<sup>1,a</sup>, Yogita Kalra<sup>1,b</sup>, Kamal Kishor<sup>1,c</sup>, and Nishant Shankhwar<sup>2,d</sup>

<sup>1</sup> Advanced Simulation Lab, Centre of Relevance and Excellence in Fiber Optics and Optical Communication, Delhi Technological University, Delhi 110042, India

<sup>2</sup> Hansraj College, University of Delhi, Delhi 110007, India

Received 20 October 2022 / Accepted 16 February 2023 / Published online 15 March 2023  
© The Author(s), under exclusive licence to EDP Sciences, SIF and Springer-Verlag GmbH Germany, part of Springer Nature 2023

**Abstract.** Plasmonics is widely used for converting electromagnetic radiation into energy and confining electromagnetic radiation below the diffraction limit. However, the ultra narrowband and high electromagnetic field cannot be obtained simultaneously because of resistive loss and radiation damping in the metals. In this article, a metallic ultra-narrow band perfect absorber has been proposed consisting of an array of four squares on a silver layer. The structure shows more than 99% absorption and full width at half maxima less than 2 nm at resonance wavelength. The absorption mechanism has been revealed by calculating electric and magnetic field profiles. The dependence of the structure on the geometrical parameters has been studied and the structure has thus been optimized at 692 nm i.e. in the visible range of frequency. The proposed structure is then investigated for sensing application. The structure shows high sensitivity of 680 nm/RIU in the visible range of wavelength and a high figure of merit of 348.72.

## 1 Introduction

Plasmonic materials have attracted much attention in previous years for varying applications in biosensors [1], optical filters [2], and photodetectors [3]. Collective oscillation of free electrons on the surface of metal due to an external electric field is known as localized surface plasmons [4]. The charges/plasmons accumulated at the opposite ends of the nanoparticle. If gap is created between the two nanoparticles, then it is evident that the order of magnitude of surface plasmons is more in the gap region rather than in the vicinity of elongated nanoparticles [5]. By choosing shape and size, amplitude and bandwidth of resonance wavelength can be controlled. This resonance wavelength also varies with the refractive index of the surrounding environment. This property can be utilised in the sensing application [6]. Plasmonic metamaterials due to localised surface plasmon convert far-field radiation into localised energy or vice-versa. Hence, they can be used in the design of optical antennas [7]. High field enhancement can be obtained in the gap region of plasmonic nanoantennas [8].

On account of being made of metals, plasmonic nanoantennas exhibit substantial ohmic loss, which facilitates their utilisation for absorption of light [9]. By choosing a suitable design and optimising geometrical parameters one can obtain absolute absorption in a range of frequencies, which can be very useful in device applications [10].

Absorbers can be categorized into broadband and narrowband on the basis of bandwidth. Broadband absorbers can be used in solar panels utilized in solar energy harvesting [11, 12]. Narrowband absorbers can be used in sensing [13–15], thermal radiation tailoring [16], absorption filters [17] etc. The first absorber was proposed and demonstrated experimentally by Lardy et al. in 2008 for sensing application in the infrared region [18]. In this design like most of the previous designs, triple layers of metal-dielectric-metal (MDM) have been chosen where a dielectric spacer enables strong plasmonic coupling between the top resonator and bottom metal film [19–21]. The above-mentioned absorbers can be considered as resonators coupled to a transmission line with a dielectric spacer region, whose thickness influences the radiative damping rates and resonance frequency. However, due to strong radiative damping and inherent metal loss, the bandwidth of the absorbers is relatively broad ( $> 40$  nm). Sensitivity and Figure of Merit (FOM) are the two important parameter to specify the performance of sensors. Sensitivity is measure of change in the output quantity with respect

<sup>a</sup> e-mail: [ritikaranga821@gmail.com](mailto:ritikaranga821@gmail.com)

<sup>b</sup> e-mail: [dryogitakalra@gmail.com](mailto:dryogitakalra@gmail.com) (corresponding author)

<sup>c</sup> e-mail: [kishorkamall@rediffmail.com](mailto:kishorkamall@rediffmail.com)

<sup>d</sup> e-mail: [nishant.shankhwar@gmail.com](mailto:nishant.shankhwar@gmail.com)

to change in the input quantity. The term "bulk sensitivity" refers to the shift in the resonance wavelength with respect to the surrounding refractive index that is used to calculate the sensitivity of the presented plasmonic sensors [22–24]. Higher FOM indicates a high ability to sense changes in the environment. It is defined by the ratio of the sensitivity to the bandwidth at half maxima of the peak. Therefore, attempts have been made to reduce the absorption bandwidth in order to increase the corresponding figure of merit (FOM). In 2016, Z. Yong et al. proposed a narrow band absorber for sensing application of FWHM 7.5 nm in the near IR region with FOM 110/RIU [25]. Many absorbers from UV to near IR have been demonstrated till now [20, 26–28]. However, narrowband absorbers in visible range have not been studied much. Most of them show resonance in a broad range of wavelengths and have a very low FOM [10, 15, 29]. Much work has been done by researchers practically and experimentally to obtain high FOM in the visible range. In 2014, Emiko and Tetsu experimentally studied localised surface plasmon resonance sensors based on spectral dips [30]. G. Liu et al. in 2016 proposed theoretically a network type plasmonic nanostructure with multiple reflection bands reaching full width at half maximum of 3 nm and FOM of 68.57/RIU [31]. In 2017, Wu et al. proposed grating absorbers with nanoribbons in between metal dielectric metal (MDM) having sensing applications in the visible range and FOM equal to 233.5/RIU [32]. In 2020, a narrow band perfect absorber of  $\text{Al}_2\text{O}_3$  based on dielectric-dielectric-metal configuration was proposed by M. Pan et al. having a sensitivity of 108 nm/RIU reaching FOM up to 240.7/RIU [33].

In this article, all metallic plasmonic narrowband absorber has been designed. The design confines and enhances electric as well as magnetic field at a single hot spot and shows a narrow absorption peak of full width at half maximum (FWHM) less than 2 nm in the visible wavelength. The design shows the sensitivity of 680 nm/RIU and FOM of 348.72/RIU, which is higher than the earlier reported results in the visible wavelength [25, 30–33]. Further, the performance of the absorber has been investigated by varying geometrical parameters and the design is optimised for maximum absorption and high FOM. The mechanism of absorption has been revealed by observing electric and magnetic field profiles. The proposed design holds great potential for sensing and near-field optics.

## 2 Design and modelling

The geometry comprises of four cuboids of silver, facing each other at tips, placed over a silver layer of thickness ( $t$ ) of 100 nm. The whole structure is placed on a glass substrate and surrounded by air on top. The design and geometrical parameters are demonstrated in Fig. 1. Length and width of cuboids have been taken as 'a' and height has been taken as 'h'. The gap 'g' between the tips of the opposite cuboid has been taken as 30 nm.

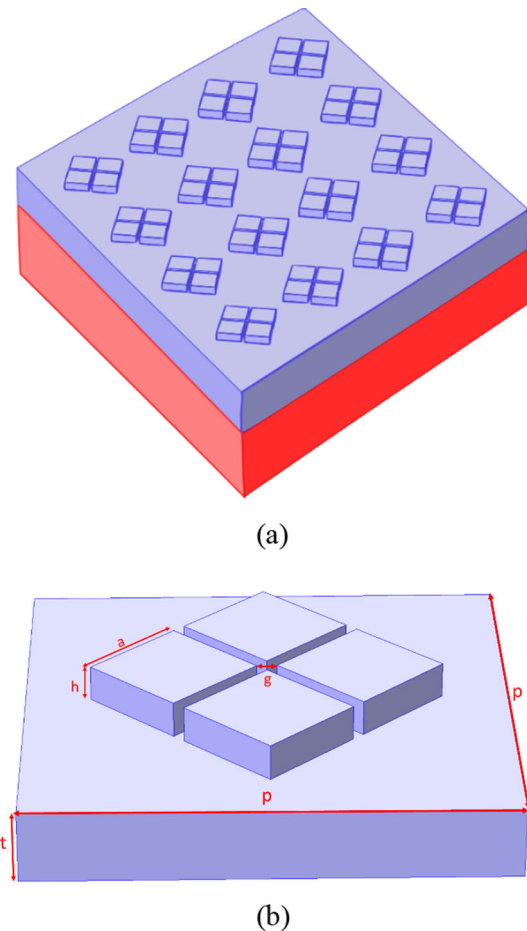


**Fig. 1** a Schematic of the proposed metallic absorber, b unit cell with geometrical parameters

The set of four cuboids has been arranged in the form of an array of periodicity 'p'.

Silver has been chosen as the material because of its high reflectivity. The thickness of the silver layer has been chosen such that no light is transmitted through this layer and the maximum absorption takes place at resonance wavelength. The value of relative permittivity for silver has been taken from literature [34].

The transverse magnetic (TM) light, polarised along x-direction is allowed to fall on the surface of the structure from the top. The distance between light source and the structure is taken more than half of resonant wavelength. The simulation is performed on single unit enclosed in a cuboid having dimensions of periodicity, p along x and y axis. The periodic boundary conditions have been applied along x and y plane on the boundary of cuboid enclosing unit cell to represent as infinite array in x–y plane. The refractive index of glass substrate is taken to be 1.5. The maximum mesh size is taken as 10 nm. The reflection coefficient has been calculated using the finite element method via COMSOL Multiphysics. The absorption coefficient has been obtained by using relationship  $A = 1 - R$ .

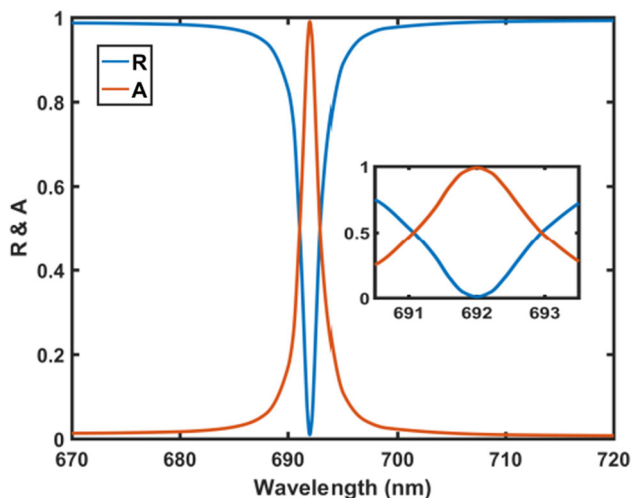


**Fig. 2** Refraction and absorption coefficient for  $a = 140$  nm,  $h = 30$  nm and  $p = 650$  nm showing resonance at 692 nm and FWHM = 1.95 nm

The resonance wavelength of plasmonic structures depends upon shape, size, geometry, constituting material as well as the surrounding medium. This property of changing resonance wavelength with refractive index can be used in sensing applications. The sensors are characterised by their sensitivity and FOM. Sensitivity,  $S$  for refractive index sensor is defined by the ratio of the spectral shift with the change of refractive index of the surrounding medium and FOM is the ratio of sensitivity to the FWHM [22–24].

$$S = \frac{\Delta\lambda}{\Delta n} \quad \text{FOM} = \frac{S}{\text{FWHM}}$$

### 3 Results and discussion

Absorption and reflection spectra for the structure has been shown in Fig. 2. As the thickness of the silver film is greater than the skin depth, the absorption is reduced to  $A = 1 - R$ . The absorption spectrum shows an absorption peak at 692 nm of which the full width at half maxima is 1.95 nm, which is much narrower than the previously reported design in the visible range [10, 15, 29–31]. A maximum of 99.45% absorption is obtained at the resonance wavelength. Further, the quality factor  $Q$  given by the ratio of the resonance wavelength to the FWHM of resonance peak ( $\lambda_{\text{res}}/\Delta\lambda$ ) which comes out to be 354.87 is much higher than previously reported designs [25, 30–33].

#### 3.1 Effect of length of the nanoantenna

##### 3.1.1 Effect of height, ‘h’

The study of dependence of the size of cuboidal pillars on the absorption peak has been studied. First,

the height of the silver cuboids has been varied, and the periodicity and sides of cuboids have been fixed at 650 nm and 160 nm respectively. The plot showing the variation of absorption coefficient and FWHM with the variation of height from 25 to 45 nm in the step of 5 nm, has been depicted in Fig. 3a and the variation of resonance wavelength with height has been shown in Fig. 3b. As there is a vertical waveguide in between four silver pillars, the increment in the height eventually increases the length of the waveguide. Therefore, the resonance shifts toward longer wavelengths, as seen in Fig. 3b. Although FWHM decreases with a decrease in the height of silver pillars, but below 30 nm height, the absorption decreases. Hence, the height has been fixed at 30 nm. Further, the effect of height of the pillars on the sensitivity has been studied by keeping all other parameters same as above and corresponding FOM has been calculated. The graph showing variation of the sensitivity and FOM of the structure with the variation in height of the nanopillars of the nanoantennas has been shown in Fig. 3c. It has been observed from the figure that there is no effect of height of the nanopillars on the sensitivity of structure but there is fall in the FOM of the structure with increase in the height because of increase in the value of FWHM with the height of nanopillars.

An increase in the value of parameter ‘h’ increases the absorption. The increase in the values of ‘h’ increases the volume of cuboidal pillars on the silver layer. This increases the regions of high E-field alongside the wall of the cuboidal pillars. The increase in the high E-field regions increases the shift in the plasmon resonance wavelength Fig. 3b. However, a higher value of ‘h’ also reduces the probability of coupling surface plasmons on top of the cuboid pillars as the evanescent tail of the plasmon will no longer be able to reach the top surface [23]. This may reduce the values of sensitivity. The FWHM is increasing with height resulting in a constant sensitivity. To achieve higher absorption, sensitivity and FOM, the height ‘h’ was adopted as 30 nm.

##### 3.1.2 Effect of side length, ‘a’

Further, the sides of silver cubes have varied from 120 to 160 nm in the step size of 10 nm, keeping the periodicity and height of cuboids at 650 nm and 30 nm respectively. The effect of varying sides of cubes on absorption coefficient and FWHM has been shown in Fig. 4a and the shift in the resonance wavelength has been shown in Fig. 4b. It has been observed that with the increase in ‘a’, there is a slight redshift in the resonance wavelength, and full width at half maxima decreases. Red shift in the resonance wavelength with the increase in side length ‘a’ can be understood in analogy to a half-wave dipole antenna whose resonant wavelength is directly proportional to antenna length, given by,

$$\lambda_{\text{resonance}} = 2 \times \text{length}$$

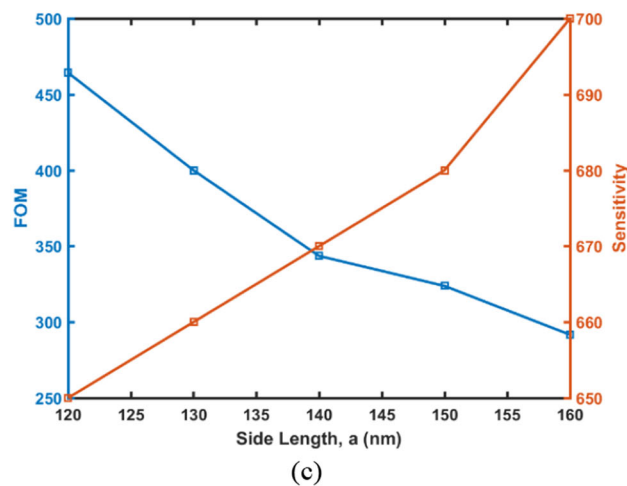
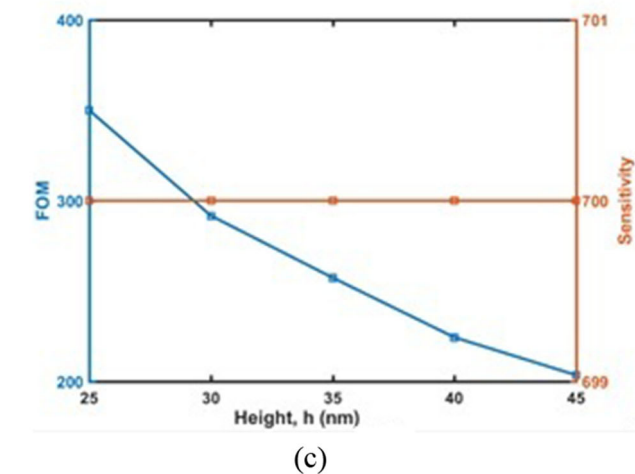
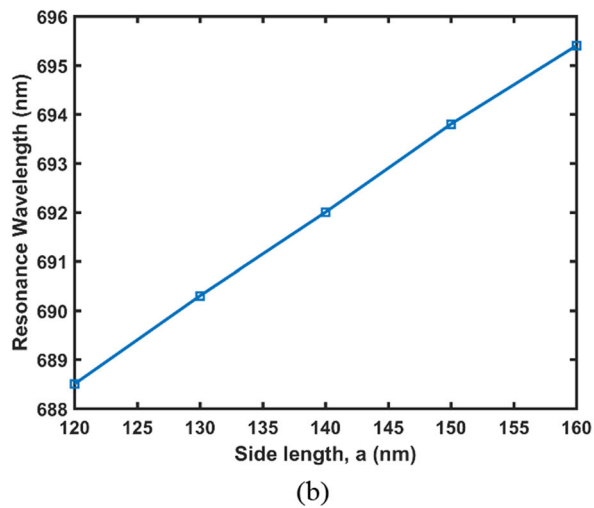
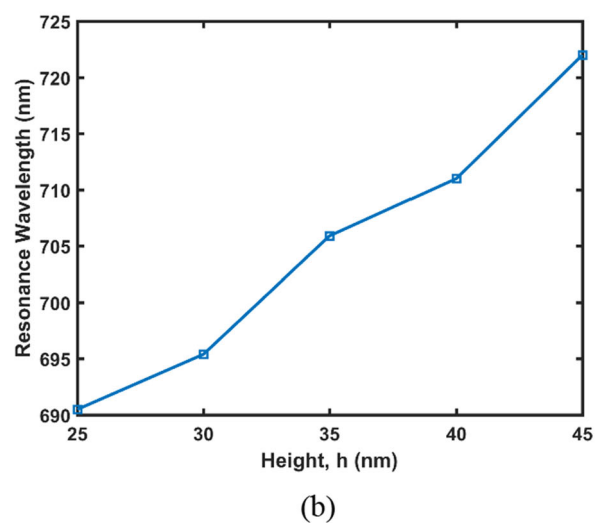
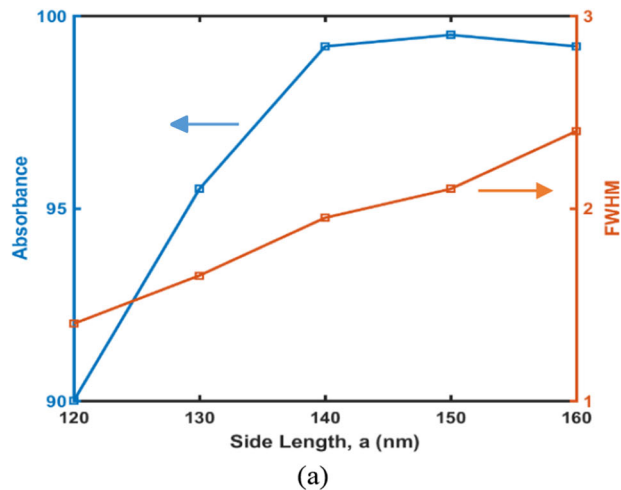
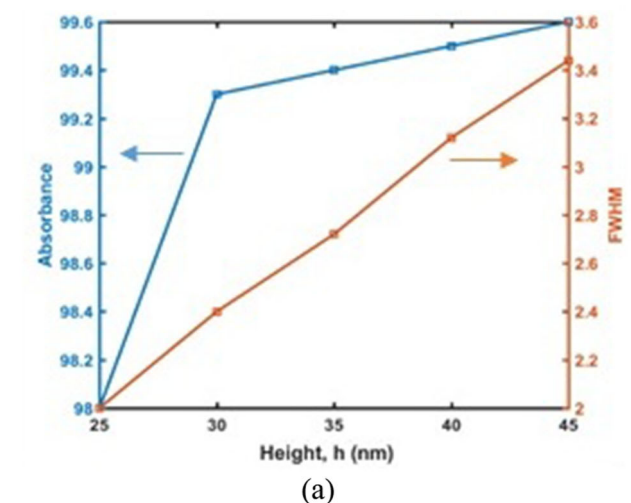


**Fig. 3** Variation of **a** absorption coefficient and FWHM, **b** resonance wavelength and **c** FOM and sensitivity with the variation of height, ‘ $h$ ’

**Fig. 4** Variation of **a** absorption coefficient and FWHM, **b** resonance wavelength and **c** FOM and sensitivity with the variation of sides of pillars, ‘ $a$ ’

As the length of the dipole increase so does the resonant wavelength [8]. In fact, it can be established as a general truth for all the antenna designs that increase in

the size of the resonant components results in increase or red shift in the resonant wavelength. Hence, in the

reported design the resonant wavelength increases with increase in side length ‘a’.

A small value of FWHM can lead to high FOM for sensing applications which can be achieved by decreasing the side lengths of pillars. But if side length is reduced below 140 nm, absorption decreases. The effect of sides of nanopillars, ‘a’ on the sensitivity and FOM of the structure can be illustrated from Fig. 4c. Sensitivity of the structure increase with increase in ‘a’ while FOM decreases with increase in ‘a’. This is because increase in value of FWHM is more than the increase in the value of sensitivity with ‘a’.

### 3.1.3 Effect of periodicity, ‘p’

Keeping ‘a’ and ‘h’ constant at 140 nm and 30 nm respectively, the periodicity of the structure has been varied from 600 nm to 800 nm in the step size of 50 nm, and absorbance and FWHM have been recorded. The variation of maximum absorption and FWHM with the variation of periodicity ‘p’ has been shown in Fig. 5a. It has been observed from the figure that FWHM decreases with an increase in periodicity and the absorption coefficient first increases then starts decreasing with a further increasing in the periodicity. Also, there is a linear shift in the resonance wavelength with an increase in periodicity as shown in Fig. 5b. The design is optimised at a wavelength of 692 nm to operate in the visible spectrum. The value of the sensitivity and the FOM has been calculated and plotted in Fig. 5c. It can be clearly shown from the Fig. 5c that both the sensitivity and FOM increases with increase in periodicity ‘p’. The shifting of the resonance wavelength with the variation of a period can be explained by using LC model. When the period decreased, the gap between adjacent unit cells will also decrease and then the E-field enhancement capacitance between adjacent unit cells will increase. So, the resonance wavelength will shift towards a higher value [6, 23, 35, 36].

### 3.1.4 Effect of gap, ‘g’

Keeping ‘a’ and ‘h’ constant at 140 nm and 30 nm respectively and the periodicity ‘p’ of the structure at 650 nm, the gap ‘g’ between the opposite two pillars has been varied from 20 to 60 nm in the step of 10 nm. The absorbance and FWHM has been calculated and plotted in Fig. 6a. It has been observed from the figure that there is maximum absorption at the gap of 30 nm while there is no effect of gap ‘g’ on the FWHM. There is slight shift in the resonance wavelength with the gap ‘g’ as observed from Fig. 6b. The variation of the sensitivity and FOM with gap ‘g’ is shown in Fig. 6c. It can be stated that there is no effect on sensitivity of the structure with the gap between the opposite pillars. Therefore, FOM remain unaltered with the gap ‘g’ as both the sensitivity and FWHM remains constant with the gap ‘g’.

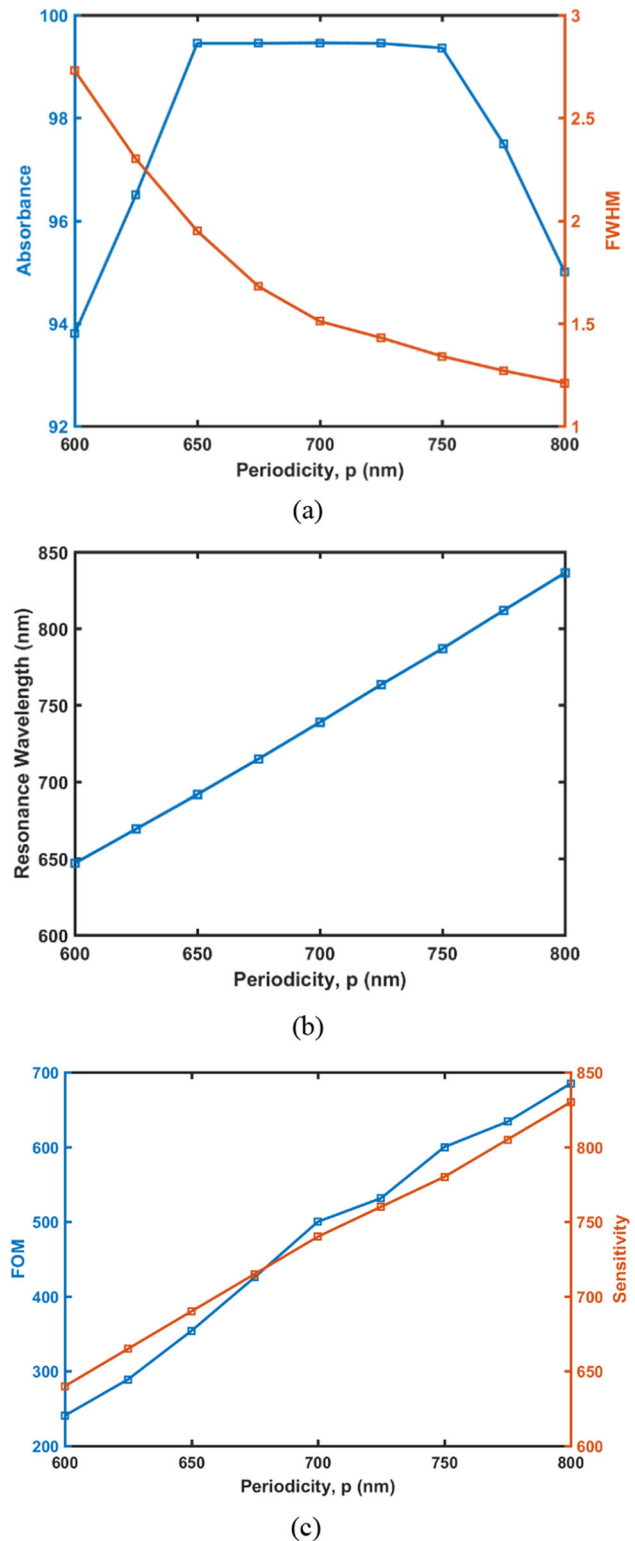
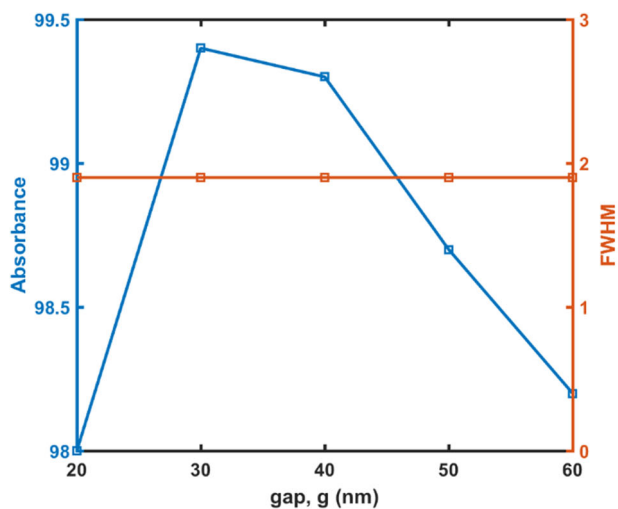
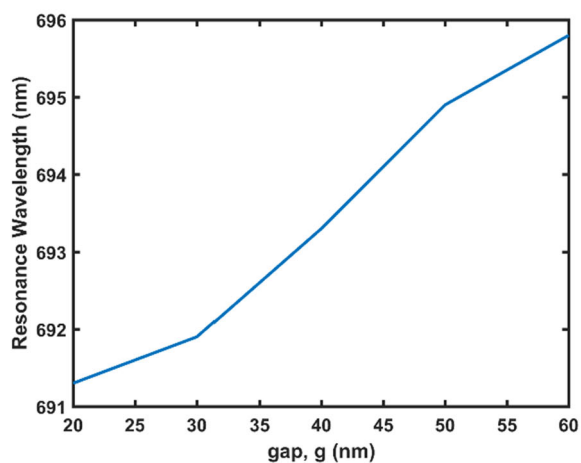


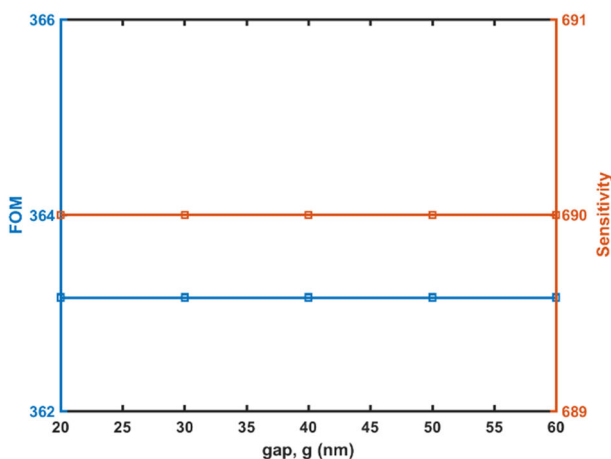
**Fig. 5** Variation of **a** Absorption coefficient and FWHM, **b** resonance wavelength and **c** FOM and sensitivity with the variation of periodicity, ‘p’



(a)

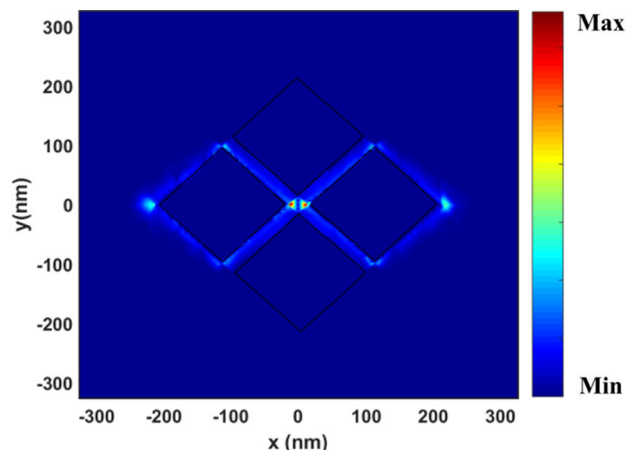


(b)

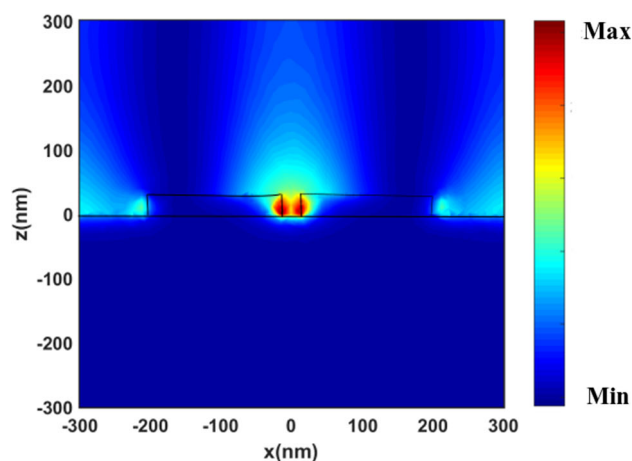


(c)

**Fig. 6** Variation of **a** absorption coefficient and FWHM, **b** resonance wavelength and **c** FOM and sensitivity with the variation of gap, 'g' between opposite pillars



(a)



(b)

**Fig. 7** **a** Distribution of electric field intensity along x–y plane, **b** distribution of magnetic field intensity along xz plane

### 3.2 Mechanism

To better understand the mechanism of absorption, electric and magnetic field spatial distribution plots have been drawn. Here geometrical parameters are set as  $a = 140$  nm,  $h = 30$  nm,  $g = 30$  nm and  $p = 650$  nm. The plane polarized light of wavelength 692 nm is allowed to fall on the absorber from the top. The corresponding electric field and magnetic field distribution has been drawn in the xy and xz plane respectively and shown in Fig. 7a, b. It has been observed from the figure that structure is not only a perfect absorber but also enhances the electric field intensity which is desirable in bio-sensors. The Fig. 7 shows that electric and magnetic fields are concentrated at the central gap. The electric field is observed due to the formation of localised surface plasmons. Localised surface plasmons tend to accumulate at the tip or the edges, that's why they are concentrated at the upper part more than the base of the cuboids. Electric field enhancement is more

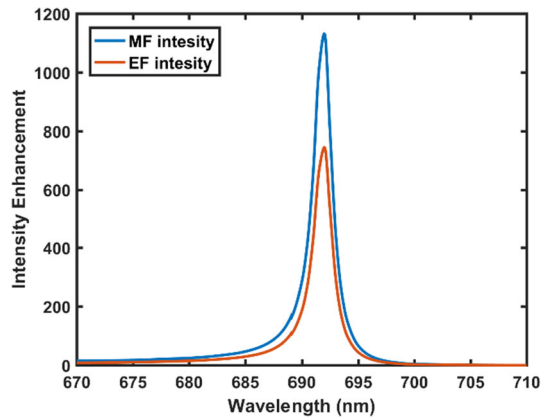


**Fig. 8** Electric and magnetic field intensity enhancement at the central gap at a height of 30 nm above the silver film

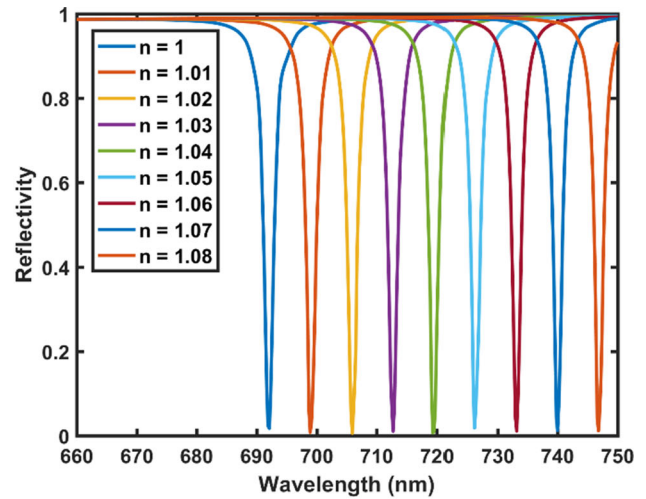
at the gap rather than the other edges. Two opposite silver pillars and the connecting silver base together act as a split ring resonator. The charges accumulated at the edges flow through the conducting base, exhibiting a current carrying loop type configuration, which results in the induction of the magnetic field in the central gap. Therefore, the magnetic field is mainly concentrated at the center of the vertical gap. Figure 7a shows the electric field intensity distribution profile from the top view and Fig. 7b shows the magnetic field intensity distribution from the side view. Both electric, as well as magnetic fields, are concentrated at the same hot spot. Figure 8 shows the electric field and magnetic field enhancement for the same configuration as mentioned above at the center of the four pillars at height of 30 nm from the silver layer, where both the curves show a narrow resonance peak.

### 3.3 Plasmonic sensing capability

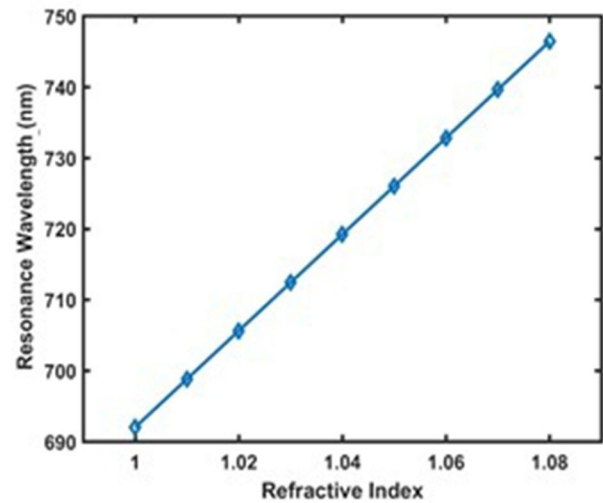
As discussed, the resonance wavelength of plasmonic structures depends upon shape, size, geometry, constituting material as well as the surrounding medium. This property of changing resonance wavelength with refractive index can be used in sensing applications. The sensors are characterised by their sensitivity and FOM. Sensitivity,  $S$  for refractive index sensor is defined by the ratio of the spectral shift with the change of refractive index of the surrounding medium, and FOM is the ratio of sensitivity to the FWHM [22–24].

$$S = \frac{\Delta\lambda}{\Delta n} \quad \text{FOM} = \frac{S}{\text{FWHM}} \quad S^* = \frac{\Delta I}{\Delta n} \quad \text{FOM}^* = \left[ \frac{S^*}{I} \right]_{max}$$

Moreover, the change of intensity is also considered for sensing as the refractive index of the surrounding environment changes.  $S^*$  is defined by the maximum change of intensity of reflected light with a unit change in refractive index.  $I$  is the absolute intensity of reflected light at resonance wavelength.  $\text{FOM}^*$  is defined by the maximum  $S^*/I$  ratio.



(a)



(b)

**Fig. 9** **a** Reflection spectrum of the proposed all metallic absorber with the variation of wavelength for different values of refractive index varying from 1 to 1.08. **b** Shift in resonance wavelength with variation of refractive index

Air like reflective index sensors with values ranging from 1 to 1.08 are most commonly used in gas sensors [6]. The optimized design has been investigated for air-like refractive index sensor for the different values of surrounding refractive index. The refractive index of the surroundings has varied from 1 to 1.08 and corresponding absorption spectra were recorded. The reflection spectrum for different values of refractive index varying from 1 to 1.08 has been shown in Fig. 9a. The variation in resonance wavelength with the variation of the refractive index of the surrounding medium has been shown in Fig. 9b. There is a redshift in the resonance wavelength with an increase in the refractive index of the surrounding. The sensitivity and FOM come out to be 680 nm/RIU and 348.72/RIU. The value of  $S^*$  and  $\text{FOM}^*$  as calculated at 692 nm comes out to be 99.68 and 17,580.

## 4 Conclusion

Ultra narrow-band perfect absorber structure has been designed and optimised. Further, this ultra-narrowband absorber will be used in refractive index sensing applications. The structure offers 99.45% absorption and has a very narrow peak at resonance wavelength. The mechanism of absorption has been revealed via observing electric and magnetic field distribution. The structure offers a high-quality factor of 354.87. The structure shows a good sensing capability with a sensitivity of 680 nm/RIU and a high figure of merit of 348.72/RIU.

**Acknowledgements** The authors gratefully acknowledge the initiatives and support provided by the establishment of the TIFAC-Centre of Relevance and Excellence in Fiber Optics and Optical Communication at Delhi Technological University (Formerly Delhi College of Engineering) Delhi, through the “Mission REACH” program of Technology Vision-2020 of the Government of India.

## Author's contribution

All authors have contributed equally to the paper.

**Data Availability Statement** This manuscript has no associated data or the data will not be deposited. [Authors' comment: There are no associated data available.]

## References

1. A.M. Shrivastav, U. Cvelbar, I. Abdulhalim, *Commun. Biol.* **4**(1), 70 (2021)
2. M.N. Baitha, K. Kim, *IEEE Photonics Technol. Lett.* **34**(24), 1329–1332 (2022)
3. A. Dorodnyy, Y. Salamin, P. Ma, J.V. Plestina, N. Lassaline, D. Mikulik, P. Romero-Gomez, A.F. i-Morrall, J. Leuthold, *IEEE J. Sel. Top. Quantum Electron.* **24**(6), 1–13 (2018)
4. H. Reather, *Springer Tracts in Modern Physics*, vol. 111 (1988), pp. 1–3.
5. A.A. Maradudin, J.R. Sambles, W.L. Barnes, *Modern Plasmonics* (Elsevier, Amsterdam, 2014)
6. S. Pevec, D. Donlagic, Miniature fiber-optic Fabry–Perot refractive index sensor for gas sensing with a resolution of  $5 \times 10^{-9}$  RIU. *Opt. Express* **26**(18), 23868–23882 (2018)
7. S. Verma, B. Rahman, *Sensors* **23**(3), 1290 (2023)
8. A.E. Krasnok, I.S. Maksymov, A.I. Denisyuk, P.A. Belov, A.E. Miroshnichenko, C.R. Simovski, Y.S. Kivshar, *Phys. Usp.* **56**(6), 539 (2013)
9. R. Ranga, Y. Kalra, K. Kishor, *Opt. Commun.* **481**, 126511 (2021)
10. P. Agarwal, K. Kishor, R.K. Sinha, *Opt. Commun.* **522**, 128667 (2022)
11. Y. Wang, T. Sun, T. Paudel, Y. Zhang, Z. Ren, K. Kempa, *Nano Lett.* **12**(1), 440–445 (2012)
12. C. Fei-Guo, T. Sun, F. Cao, Q. Liu, Z. Ren, *Light Sci. Appl.* **3**(4), e161 (2014)
13. Y. Li, L. Su, C. Shou, C. Yu, J. Deng, Y. Fang, *Sci. Rep.* **3**(1), 2865 (2013)
14. A.A. Jamali, B. Witzigmann, *Plasmonics* **9**, 1265–1270 (2014)
15. W. Zhou, K. Li, C. Song, P. Hao, M. Chi, M. Yu, Y. Wu, *Opt. Express* **23**(11), A413–A418 (2015)
16. X. Liu, T. Tyler, T. Starr, A.F. Starr, N.M. Jokerst, W.J. Padilla, *Phys. Rev. Lett.* **107**(4), 045901 (2011)
17. K.T. Lee, S. Seo, L.J. Guo, *Adv. Opt. Mater.* **3**(3), 347–352 (2015)
18. N.I. Landy, S. Sajuyigbe, J.J. Mock, D.R. Smith, W.J. Padilla, *Phys. Rev. Lett.* **100**(20), 207402 (2008)
19. Q. Li, Z. Li, X. Xiang, T. Wang, H. Yang, X. Wang, Y. Gong, J. Gao, *Coatings* **9**(6), 393 (2019)
20. J. Becker, A. Trügler, A. Jakab, U. Hohenester, C. Sönnichsen, *Plasmonics* **5**, 161–167 (2010)
21. C. Huang, J. Ye, S. Wang, T. Stakenborg, L. Lagae, *Appl. Phys. Lett.* **100**(17), 173114 (2012)
22. A.K. Agrawal, A. Ninawe, A. Dhawan, *IEEE Sens. J.* **22**(7), 6491–6508 (2021)
23. A.K. Agrawal, A. Suchitta, A. Dhawan, *RSC Adv.* **12**(2), 929–938 (2022)
24. A.K. Agrawal, A. Suchitta, A. Dhawan, *IEEE Access* **9**, 10136–10152 (2021)
25. Z. Yong, S. Zhang, C. Gong, S. He, *Sci. Rep.* **6**(1), 24063 (2016)
26. N. Liu, M. Mesch, T. Weiss, M. Hentschel, H. Giessen, *Nano Lett.* **10**(7), 2342–2348 (2010)
27. D. Wu, Y. Liu, R. Li, L. Chen, R. Ma, C. Liu, H. Ye, *Nanoscale Res. Lett.* **11**(1), 1–9 (2016)
28. S. Luo, J. Zhao, D. Zuo, X. Wang, *Opt. Express* **24**(9), 9288–9294 (2016)
29. S.-Y. Cho, J.L. Briscoe, I.A. Hansen, J.K. Smith, Y. Chang, I. Brener, *IEEE Sens. J.* **14**(5), 1399–1404 (2013)
30. E. Kazuma, T. Tatsuma, *Nanoscale* **6**(4), 2397–2405 (2014)
31. G. Liu, M. Yu, Z. Liu, P. Pan, X. Liu, S. Huang, Y. Wang, *Plasmonics* **11**, 677–682 (2016)
32. D. Wu, R. Li, Y. Liu, Z. Yu, L. Yu, L. Chen, C. Liu, R. Ma, H. Ye, *Nanoscale Res. Lett.* **12**(1), 1–11 (2017)
33. M. Pan, Z. Su, Z. Yu, P. Wu, H. Jile, Z. Yi, Z. Chen, *Results Phys.* **19**, 103415 (2020)
34. P.B. Johnson, R.-W. Christy, *Phys. Rev. B* **6**(12), 4370 (1972)
35. Z. Ma, F. Ding, Ultra-broadband metamaterial absorber in Terahertz regime, in *2012 Asia Communications and Photonics Conference (ACP)*, 7–10 Nov. 2012 (2012), pp. 1–3.
36. B.-X. Wang, X. Zhai, G.-Z. Wang, W.-Q. Huang, L.-L. Wang, *J. Appl. Phys.* **117**(1), 014504 (2015)

Springer Nature or its licensor (e.g. a society or other partner) holds exclusive rights to this article under a publishing agreement with the author(s) or other rightsholder(s); author self-archiving of the accepted manuscript version of this article is solely governed by the terms of such publishing agreement and applicable law.